Structural properties of amorphous $GeSe_2$

2007 J. Phys.: Condens. Matter 19 415111

(http://iopscience.iop.org/0953-8984/19/41/415111)

IOP PUBLISHING JOURNAL OF PHYSICS: CONDENSED MATTER

J. Phys.: Condens. Matter **19** (2007) 415111 (9pp) doi:10.1088/0953-8984/19/41/415111

Structural properties of amorphous $GeSe_2$

Carlo Massobrio[1] **and Alfredo Pasquarello**[2,3]

[1] Institut de Physique et de Chimie des Matériaux de Strasbourg, 23 rue du Loess, BP43, F-67034 Strasbourg Cedex 2, France
[2] Ecole Polytechnique Fédérale de Lausanne (EPFL), Institute of Theoretical Physics, CH-1015 Lausanne, Switzerland
[3] Institut Romand de Recherche Numérique en Physique des Matériaux (IRRMA), CH-1015 Lausanne, Switzerland

Received 2 May 2007, in final form 6 June 2007
Published 27 September 2007
Online at stacks.iop.org/JPhysCM/19/415111

Abstract

By using first-principles molecular dynamics within density functional theory, we study the structural properties of amorphous $GeSe_2$ at $T = 300$ K. The amorphous configurations have been obtained via cooling from the liquid state followed by extensive relaxation (22 ps) at $T = 300$ K. The agreement with neutron diffraction experiments is very satisfactory, in particular for the pair correlation functions in real space and the partial structure factors in reciprocal space describing the Ge–Se and the Se–Se correlations. Some residual differences between theory and experiment are found for Ge–Ge correlations. The network organizes itself through the predominant presence of $GeSe_4$ tetrahedra. However, other coordinations exist in non-negligible proportions for both Ge and Se. Homopolar bonds are found for Se, and, in a very limited extent, also for Ge. The number of edge-sharing connections reproduces the experimental data.

1. Introduction

Network-forming disordered systems of stoichiometry AX_2 (A: Si, Ge; X: O, S, Se) share the predominant presence of the AX_4 tetrahedron as the main building block and the occurrence of intermediate-range order [1, 2]. This extended degree of structural organization manifests itself through the appearance of a first sharp diffraction peak (FSDP) in the total neutron structure factor [1, 2]. Despite these similarities, the atomic structures of AX_2 glasses can differ considerably as a result of variations in the nature of the A–X bonding. This concept is exemplified by the observation that the highly ionic amorphous SiO_2 is an undefective network of corner-sharing tetrahedra, while the less ionic amorphous $GeSe_2$ (a-$GeSe_2$) significantly departs from chemical order [3–6]. For a-$GeSe_2$, compelling evidence in this direction was obtained through a series of measurements carried out with the method of isotopic substitution in neutron diffraction [6, 7]. Salmon and co-workers have described a-$GeSe_2$ as a defective network made of close proportions of corner- and edge-sharing connections. Partial structure

factors $S_{\alpha\beta}(k)$ in reciprocal space and pair correlation functions $g_{\alpha\beta}(r)$ in direct space were measured [6, 7]. Chemical disorder was quantified in terms of Ge–Ge and Se–Se homopolar bonds [6, 7]. A reliable modelling of a-$GeSe_2$ has been a challenge for atomic-scale studies of materials since the late 1980s[4]. Early approaches failed to predict miscoordinations and homopolar bonds (see footnote 4). To improve the description of these aspects, several investigations have been stimulated, including the use of approximate density functional schemes or of interatomic potentials derived from first-principles calculations[5].

In this paper, first-principles molecular dynamics in the framework of density functional theory is employed to calculated partial structure factors $S_{\alpha\beta}(k)$ and pair correlation functions $g_{\alpha\beta}(r)$ of glassy $GeSe_2$. Together with a neighbour analysis this sheds light on the atomic structure of the disordered network. Our approach is substantiated by successful studies on liquid $GeSe_2$. In addition to a structural description consistent with experiments, we were able to link measured features of short- and intermediate-range order to specific constitutive units [11–16]. Here, we provide for the case of a-$GeSe_2$ indications on the level of agreement and the remaining differences between theory and experiment. A detailed account on the structural and vibrational properties of a-$GeSe_2$ based on a single model configuration at $T = 0$ K is given elsewhere [17].

This paper is organized as follows. In section 2 we describe how we generate our structure for a-$GeSe_2$. Our results are collected in two sections, devoted to the real space properties (section 3) and reciprocal space properties (section 4). Concluding remarks can be found in section 5.

2. Theoretical model

Our simulations were performed at constant volume on a system consisting of 120 atoms (40 Ge and 80 Se). We used a periodically repeated cubic cell of size 15.16 Å, corresponding to an experimental density of 0.034 $Å^{-3}$ at $T = 300$ K [18]. The electronic structure was described within density functional theory and evolved self-consistently during the motion [19, 20]. Valence electrons were treated explicitly, in conjunction with norm-conserving pseudopotentials to account for core–valence interactions. We resorted to a generalized gradient approximation [21], with norm-conserving pseudopotentials generated as in [22]. The wavefunctions are expanded at the Γ point of the supercell. The energy cutoff is taken equal to $E_c = 20$ Ryd. We refer to previous studies on liquid $GeSe_2$ for the technical ingredients of our simulations [13].

To construct our amorphous structure and achieve optimal statistical sampling, we have selected six configurations separated by 3 ps along a trajectory of 20 ps previously generated for the liquid [13]. The corresponding coordinates are rescaled to match the density of the amorphous and the six subtrajectories are followed in time. For each one of them, the system is cooled from 1100 to 600 K in 22 ps (10 ps at 1100 K, 7 ps at 900 K and 5 ps at 600 K) and further annealed for 22 ps at $T = 300$ K. First-principles molecular dynamics is performed by using Nosé–Hoover thermostats at the given target temperature [23, 24]. The interval of 22 ps in between 1100 and 600 K allowed for significant atomic diffusion after the density change. The second long interval of the same length (22 ps at $T = 300$ K) had the purpose of fully relaxing the amorphous structure. This was confirmed *a posteriori* by the structural modifications observed during the first 5 ps of this interval. Results presented in this paper

[4] For early studies of disordered $GeSe_2$ systems based on the use of effective potentials, see [8].

[5] For the application to amorphous $GeSe_2$ of a non-self-consistent electronic structure scheme based on the local density approximation and the use of a minimal basis set, see [9]. For a recent example of application to amorphous $GeSe_2$ of based on interatomic potentials derived from first-principles data, see [10].

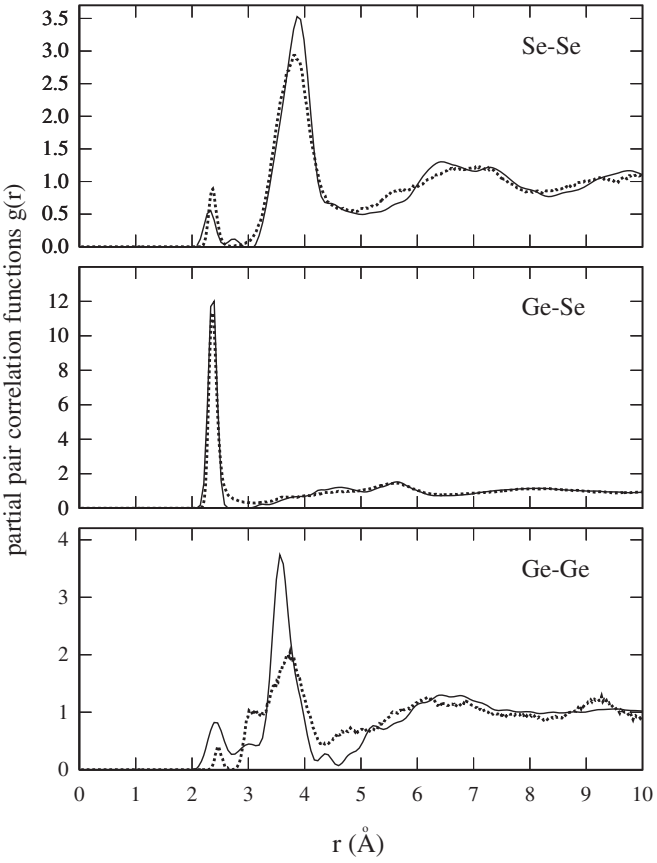

Figure 1. Pair correlation function for amorphous $GeSe_2$: our calculations (dotted line) compared with experimental data (solid line, [26]).

are temporal averages taken over the last 12 ps for a single subtrajectory at $T = 300$ K. In a further paper [25], we shall provide results obtained from global averages taken over the six subtrajectories.

3. Real-space properties

In figure 1, we display the calculated and experimental partial pair correlation functions (PCFs) $g^{\text{th}}_{\alpha\beta}(r)$. Peak positions and coordination numbers $n_{\alpha\beta}$ extracted from the PCFs are reported in table 1, where they are compared to the experimental data presented in table 2 of [7]. In the case of $g_{\text{SeSe}}(r)$, the overall shape is well reproduced by our calculations. The first peak, accounting for homopolar Se–Se bonds, is located at a 2% larger value of r than in $g^{\text{exp}}_{\text{SeSe}}(r)$ and has a higher intensity, leading to a moderate overestimate of n_{SeSe} (0.24 against 0.2). We found no sign of a second, small peak for $r < 3$ Å, as reported in [7]. The position of the main peak closely corresponds to the experimental one in $g^{\text{exp}}_{\text{SeSe}}(r)$, but the intensity of the theoretical peak is lower by 15%. For $r > 5$ Å, small differences are found between the oscillating patterns of $g^{\text{th}}_{\text{SeSe}}(r)$ and $g^{\text{exp}}_{\text{SeSe}}(r)$. For the number of neighbours, values in between 9 and 10 are found in both theory and experiment after integration on the respective ranges around the main peak (cf table 1). These are determined by the two minima preceding and following a maximum.

Table 1. First (FP), second (SP) and third (TP) peak positions in experimental [7] and theoretical $g_{\alpha\beta}(r)$. $n_{\alpha\beta}$, $n'_{\alpha\beta}$ and $n''_{\alpha\beta}$ are the corresponding coordination numbers. IR corresponds to the integration range for each coordination number. In our calculations the IRs are taken as the intervals between the two minima preceding and following a maximum, respectively. Note that we had no signature of a second peak in $g_{\mathrm{SeSe}}(r)$. For clarity, the peak position, integration range and coordination number relative to the second peak in $g_{\mathrm{SeSe}}(r)$ have been compared to the corresponding values relative to the third peak in the experimental $g_{\mathrm{SeSe}}(r)$.

$g_{\alpha\beta}(r)$	FP (Å)	$n_{\alpha\beta}$	IR[FP] (Å)	SP (Å)	$n'_{\alpha\beta}$	IR[SP] (Å)
$g^{\mathrm{exp}}_{\mathrm{GeGe}}(r)$	2.42	0.25	0–2.73	3.02	0.34	2.73–3.19
$g_{\mathrm{GeGe}}(r)$	2.45	0.05	0–2.70	3.11	0.32	2.70–3.14
$g^{\mathrm{exp}}_{\mathrm{GeSe}}(r)$	2.36	3.71	2.09–2.61			
$g_{\mathrm{GeSe}}(r)$	2.37	3.92	2.11–3.12			
$g^{\mathrm{exp}}_{\mathrm{SeSe}}(r)$	2.32	0.20	0–2.55	2.74	0.06	2.55–3.09
$g_{\mathrm{SeSe}}(r)$	2.37	0.24	0–2.70			
	TP (Å)	$n''_{\alpha\beta}$	IR[TP] (Å)			
$g^{\mathrm{exp}}_{\mathrm{GeGe}}(r)$	3.57	3.2	3.19–4.23			
$g_{\mathrm{GeGe}}(r)$	3.74	3.02	3.14–4.34			
$g^{\mathrm{exp}}_{\mathrm{SeSe}}(r)$	3.89	9.3	3.09–4.39			
$g_{\mathrm{SeSe}}(r)$	3.81	9.85	2.70–4.62			

As can be seen in figure 1, $g^{\mathrm{th}}_{\mathrm{GeSe}}(r)$ is in very good agreement with experiment in terms of the position, the intensity, and the width of the main peak. The only notable difference is a sharper decay to zero of $g^{\mathrm{exp}}_{\mathrm{GeSe}}(r)$ for $r > 2.5$ Å. This results in a higher theoretical n_{GeSe}, (3.92 against 3.71, [7]), very close to the value of 4 for a perfect tetrahedral network.

The comparison between $g^{\mathrm{th}}_{\mathrm{GeGe}}(r)$ and $g^{\mathrm{exp}}_{\mathrm{GeGe}}(r)$ reveals in both PCFs three distinct features in the region 2 Å $< r <$ 4 Å. The first and third features show up as distinct peaks, while the second feature is discernible as a shoulder. These features can be associated to homopolar Ge–Ge bonds, Ge atoms involved in edge-sharing connections, and Ge atoms involved in corner-sharing connections, respectively. In our case, the first peak is due to a single Ge_2 dimer and it determines the fraction of Ge atoms involved in homopolar bonds. The fraction obtained in the simulation ($2/40 = 5\%$) underestimates the experimental value of 25% [6, 7]. Integration of the shoulder around 3 Å provides an estimate of the number of Ge atoms in edge-sharing connections consistent with experiments (0.32 versus 0.34, [7]). This value is confirmed by the number of Ge atoms found in two (or more) fourfold rings (see table 2). The disagreement on the intensity of the main peak and the flattened shape of the next minimum further reflects current limitations in the description of Ge–Ge correlations. A discussion devoted to this issue can be found in our work on liquid $GeSe_2$ [13].

Information on the short-range structure of a-$GeSe_2$ is given in table 2. We defined $n_\alpha(l)$ as the average number of atoms of species α l-fold coordinated, where α are Ge or Se atoms. The number of Ge atoms fourfold coordinated and of Se atoms twofold coordinated is higher than in the liquid (75.6% versus 60.9% and 94.6% versus 70.3%, respectively), indicating that the chemical order is partially restored upon cooling. In addition to the tetrahedral arrangements that are largely predominant, the Ge atoms also show first-neighbour shells composed of GeSe, $GeSe_2$, $GeSe_3$ and $GeSe_5$. Two Ge atoms form one single Ge_2 dimer within a Se_3–Ge–Ge–Se_3 ethane-like unit. In the case of Se, as much as 22.4% of Se atoms are twofold coordinated with one Se and one Ge atom in the first-neighbour shell. Homopolar connections lead to 8 Se dimers plus one Se trimer. Table 2 also contains the comparison with the

Table 2. Average number $n_\alpha(l)$ (bold character, expressed as a percentage) of atoms of species α (α = Ge, Se) l-fold coordinated at a distance of 2.7 Å. For each value of $n_\alpha(l)$, we give the identity and the number of the Ge and Se neighbours. We also give the average number of dimers and trimers for the two species. Finally, we compare calculated and experimental values (in percentages) for the number of Ge–Ge homopolar bonds, $N_{\mathrm{Ge-Ge}}$, the number of Se–Se homopolar bonds, $N_{\mathrm{Se-Se}}$, the number of Ge atoms forming edge-sharing connections, $N_{\mathrm{Ge}}(\mathrm{ES})$ and the number of Ge atoms forming corner-sharing connections, $N_{\mathrm{Ge}}(\mathrm{CS})$.

Ge		$l=1$	**5.0**	$l=2$	**11.1**
		Se	5.0	GeSe	—
				Se_2	11.1
$l=3$	**5.9**	$l=4$	**75.6**	$l=5$	**1.8**
Se_3	5.9	$GeSe_3$	5.0	Ge_2Se_3	—
		Se_4	70.6	$GeSe_4$	—
				Se_5	1.8
Se		$l=1$	**2.3**	$l=2$	**94.6**
		Se	—	Se_2	1.2
		Ge	2.3	SeGe	22.4
				Ge_2	71.0
		$l=3$	**3.0**		
		Ge_3	3.0		

	Dimers	Trimers
Ge	1	—
Se	8	1

	$N_{\mathrm{Ge-Ge}}$	$N_{\mathrm{Se-Se}}$	$N_{\mathrm{Ge}}(\mathrm{ES})$	$N_{\mathrm{Ge}}(\mathrm{CS})$
This work	5	24	32	63
Reference [7]	25	20	34	41

results of [7] for the percentage number of Ge and Se atoms in homopolar bonds, $N_{\mathrm{Ge-Ge}}$ and $N_{\mathrm{Se-Se}}$, and the percentage number of Ge atoms forming edge- [$N_{\mathrm{Ge}}(\mathrm{ES})$] and corner-sharing [$N_{\mathrm{Ge}}(\mathrm{CS})$] connections. To obtain $N_{\mathrm{Ge}}(\mathrm{CS})$, we follow the criterion proposed by Salmon, i.e. $N_{\mathrm{Ge}}(\mathrm{CS}) = 1 - N_{\mathrm{Ge}}(\mathrm{ES}) - N_{\mathrm{Ge-Ge}}$, which holds in the absence of extended chains [7]. Due to our underestimation of $N_{\mathrm{Ge-Ge}}$, our calculations give corner-sharing connections in excess with respect to experiment (63% versus 41%).

4. Reciprocal-space properties

In figure 2, the calculated total neutron structure factor is compared with its experimental counterpart [26]. The results are less satisfactory than in the case of liquid $GeSe_2$ [11]. In particular, the FSDP and the second peak have lower intensities. Also, some spurious spikes in between the first three peaks are noticeable. We anticipate that some of these shortcomings are attenuated when accounting for all subaverages produced in our simulations [25].

The decomposition of the total neutron structure factor in Faber–Ziman partial structure factors $S_{\mathrm{SeSe}}(k)$, $S_{\mathrm{GeSe}}(k)$ and $S_{\mathrm{GeGe}}(k)$ is shown in figure 3. In the case of $S_{\mathrm{SeSe}}(k)$ and $S_{\mathrm{GeSe}}(k)$, theory compares very favourably to experiments over the entire k range, with a remarkable agreement for the position of the peaks and the sequence of maxima and minima. However, some of the peak intensities are different. This is the case in the FSDP region ($\sim$1 $\mathrm{Å}^{-1}$) of the calculated $S_{\mathrm{GeSe}}(k)$, where the experimental structure is not well reproduced. The situation is even less satisfactory for $S_{\mathrm{GeGe}}(k)$. Overall the theoretical $S_{\mathrm{GeGe}}(k)$ is less structured than in

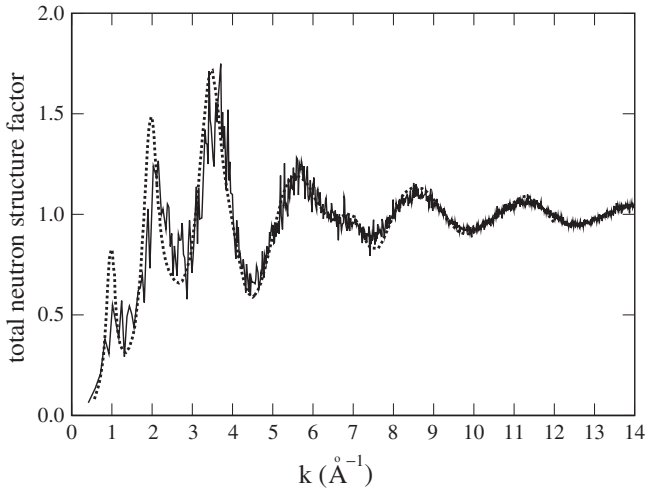

Figure 2. Total neutron structure factor of amorphous $GeSe_2$: our calculations (dotted) compared with experimental data (solid line, [6]). We used scattering lengths of $b_{Ge} = 8.189$ and $b_{Se} = 7.97$ fm [7].

the experiment. In the region 2 Å^{-1} $< k <$ 3 Å^{-1} the calculated $S_{GeGe}(k)$ is systematically lower. Furthemore, the theoretical $S_{GeGe}(k)$ does not show a pronounced minimum between the first two peaks as in the experiment, and the theoretical FSDP is lower. Concerning the latter feature, the disagreement with the experiment is nevertheless not as dramatic as in the case of liquid $GeSe_2$ [13]. In addition, the position of the FSDP is very well reproduced. Overall, it appears that the underestimate of the FSDP height in the total neutron structure factor stems from the $S_{GeSe}(k)$ and the $S_{GeGe}(k)$ contributions, which are both lower than in the experiment. The opposite occurred for liquid $GeSe_2$, where a lower FSDP in $S_{GeGe}(k)$ was compensated by a higher FSDP in $S_{GeSe}(k)$, leading to an excellent agreement between theory and experiment over the full k range for the total neutron structure factor.

In view of its sensitivity to the chemical order, it is of interest to calculate the Bhatia–Thornton [27][6] concentration–concentration partial structure factor $S_{cc}(k)$, defined as

$$S_{cc}(k) = c_{Ge}c_{Se}[1 + c_{Ge}c_{Se}((S_{GeGe}(k) - S_{GeSe}(k)) + (S_{SeSe}(k) - S_{GeSe}(k)))], \quad (1)$$

where $S_{SeSe}(k)$, $S_{GeSe}(k)$ and $S_{GeGe}(k)$ are the Faber–Ziman partial structure factors for a binary systems made of Ge and Se species at given concentrations c_{Ge} and c_{Se}, respectively. Early first-principles molecular dynamics results did not show any FSDP in the $S_{cc}(k)$ of liquid $GeSe_2$, in disagreement with experiments [11]. This disagreement has motivated several studies on the atomic-scale origins of the FSDP in the $S_{cc}(k)$. By taking into account a series of glasses and liquids, we showed that the FSDP in $S_{cc}(k)$ occurs for moderate departures from chemical order, vanishing either for high levels of structural disorder or when the chemical order is essentially perfect [14, 15]. In a further analysis, carried out on liquid $GeSe_2$, we have found that a sequence of connected fourfold rings can be taken as the structural fingerprint for the presence of an FSDP in $S_{cc}(k)$ [16].

Our calculated $S_{cc}(k)$ agrees well with its experimental counterpart (see figure 4). The calculated main peak is slightly wider than in the experiment. However, its height and position are accurately reproduced. The same holds for the FSDP, clearly discernible at the correct

[6] For the explicit relationship between the three sets of partial structure factors commonly used (Faber–Ziman, Ashcroft–Langreth and Bhatia–Thornton [27]) see [28].

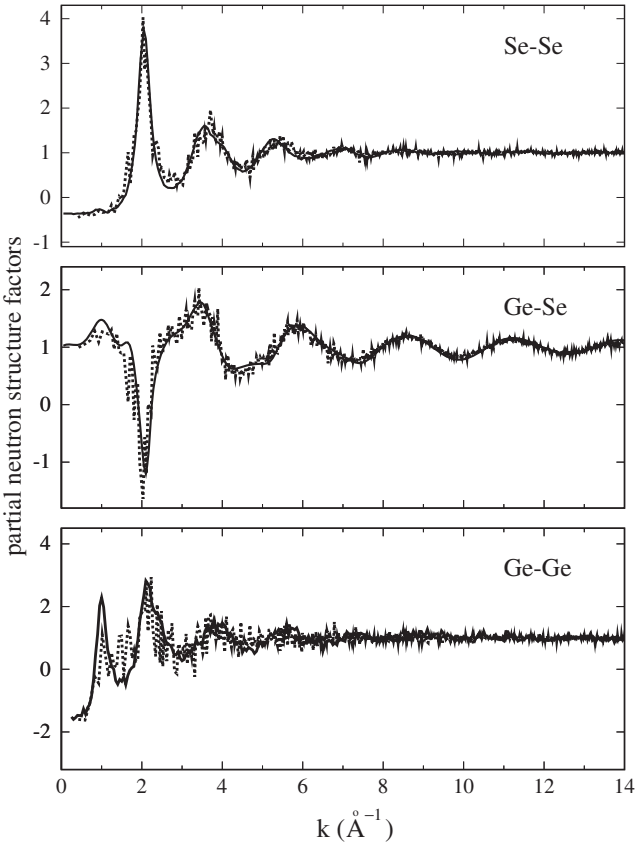

Figure 3. Faber–Ziman partial structure factors for amorphous $GeSe_2$: our calculations (dotted line) compared with experimental data (solid line, [6, 7]).

location. This accord appears as an improvement upon the case of liquid $GeSe_2$. However, the origin of this accord can be traced back to a cancellation effect involving the FSDP height of $S_{GeSe}(k)$ and $S_{GeGe}(k)$. This can be seen in figure 3 and checked by using equation (1): the difference between theory and experiment in $S_{GeSe}(k)$ is offset by that between calculated and experimental $S_{GeGe}(k)$. The presence of an FSDP in the $S_{cc}(k)$ structure factor is consistent with the previously identified relationship between a small departure from chemical order and the appearance of the FSDP. Indeed, the intensity found for the FSDP of $S_{cc}(k)$ in a-$GeSe_2$ is comparable to that of the FSDP in the $S_{cc}(k)$ of a-$SiSe_2$, a system with a moderate departure from chemical order [29].

5. Conclusions

Amorphous $GeSe_2$ can be described as a disordered network-forming material combining the predominant presence of tetrahedra and a non-negligible amount of homopolar bonds and miscoordinations. In this respect, our first-principles molecular dynamics results are fully consistent with neutron diffraction experiments. Our approach is quantitatively reliable for the case of Ge–Se and Se–Se correlations, albeit less satisfactory in predicting properties involving Ge–Ge correlations. This is expected in view of the drawbacks encountered in

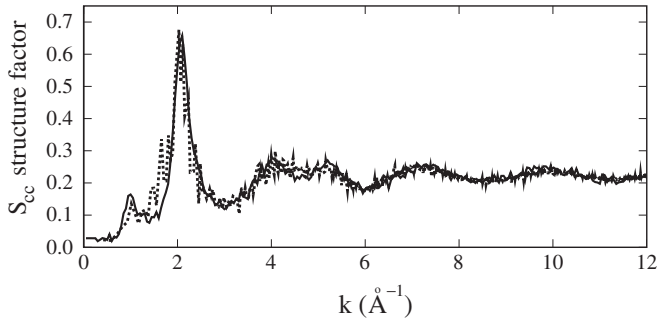

Figure 4. Bhatia–Thornton $S_{cc}(k)$ concentration–concentration partial structure factor for amorphous $GeSe_2$: our calculations (dotted line) compared with experimental data (solid line, [7]).

the case of liquid $GeSe_2$. Homopolar bonds are found for both Ge and Se. The number of edge-sharing connections is correctly recovered, while we found a larger number of corner-sharing tetrahedra, due to the underestimation of the concentration of Ge–Ge homopolar bonds. Therefore, it appears that Ge atoms do prefer to deviate from chemical order by forming groups other than $GeSe_4$ rather than forming Ge–Ge chains. Our model is able to reproduce a very elusive feature present in $GeSe_2$ disordered networks, the first sharp diffraction peak in the concentration–concentration structure factor.

From the methodological point of view, it is interesting to observe the consistent reduction of structural defects that has followed the cooling process. This is an indication of the capability of the technique to adjust to a drastic change in thermal conditions, in spite of the very high cooling rates.

Acknowledgments

We thank P S Salmon (Bath) for stimulating exchanges. The calculations were performed on the NEC-SX5 of the Swiss Center for Scientific Computing (CSCS) and on the NEC-SX5 of the IDRIS computer centre of CNRS (France).

References

[1] Elliott S R 1991 *Nature* **354** 445
[2] Moss S C and Price D L 1985 *Physics of Disordered Materials* ed D Adler, H Fritzsche and S R Ovshinsky (New York: Plenum) p 77
[3] Devine R A B (ed) 1988 *The Physics and Technology of Amorphous SiO_2* (New York: Plenum)
[4] Sarnthein J, Pasquarello A and Car R 1995 *Phys. Rev. Lett.* **74** 4682
Sarnthein J, Pasquarello A and Car R 1995 *Phys. Rev.* B **52** 12690
[5] Boolchand P and Bresser W J 2000 *Phil. Mag.* B **80** 1757
[6] Petri I, Salmon P S and Fischer H E 2000 *Phys. Rev. Lett.* **84** 2413
[7] Petri I and Salmon P S 2003 *J. Phys.: Condens. Matter* **15** S1509
[8] Vashishta P, Kalia R K, Antonio G A and Ebbsjö I 1989 *Phys. Rev. Lett.* **62** 1651
Vashishta P, Kalia R K, Rino J P and Ebbsjö I 1990 *Phys. Rev.* B **41** 12197
Iyetomi H, Vashishta P and Kalia R K 1991 *Phys. Rev.* B **43** 1726
[9] Cobb M and Drabold D A 1997 *Phys. Rev.* B **56** 3054
Zhang X and Drabold D A 2000 *Phys. Rev.* B **62** 15695
Durandurdu M and Drabold D A 2002 *Phys. Rev.* B **65** 104208
Tafen D N and Drabold D A 2003 *Phys. Rev.* B **68** 165208
Biswas P, Tafen D N and Drabold D A 2005 *Phys. Rev.* B **71** 054204

Tafen D N and Drabold D A 2005 *Phys. Rev.* B **68** 054206
[10] Mauro J C and Varshneya A K 2006 *J. Am. Ceram. Soc.* **89** 2323
[11] Massobrio C, Pasquarello A and Car R 1998 *Phys. Rev. Lett.* **80** 2342
[12] Massobrio C, Pasquarello A and Car R 1999 *J. Am. Chem. Soc.* **121** 2943
[13] Massobrio C, Pasquarello A and Car R 2001 *Phys. Rev.* B **64** 144205
[14] Massobrio C and Pasquarello A 2003 *Phys. Rev.* B **68** 020201(R)
[15] Massobrio C, Celino M and Pasquarello A 2004 *Phys. Rev.* B **70** 174202
[16] Massobrio C and Pasquarello A 2007 *Phys. Rev.* B **75** 014206
[17] Giacomazzi L, Massobrio C and Pasquarello A 2007 *Phys. Rev.* B **75** 174207
[18] Petri I and Salmon P S 2002 *Phys. Chem. Glasses* **43C** 185
[19] Car R and Parrinello M 1985 *Phys. Rev. Lett.* **55** 2471
[20] Laasonen K, Pasquarello A, Car R, Lee C and Vanderbilt D 1993 *Phys. Rev.* B **47** 10142
[21] Perdew J P, Chevary J A, Vosko S H, Jackson K A, Pederson M R, Singh D J and Fiolhais C 1992 *Phys. Rev.* B **46** 6671
[22] Dal Corso A, Pasquarello A, Baldereschi A and Car R 1996 *Phys. Rev.* B **53** 1180
[23] Nosé S 1984 *Mol. Phys.* **52** 255
Hoover W G 1985 *Phys. Rev.* A **31** 1695
[24] Blöchl P and Parrinello M 1992 *Phys. Rev.* B **45** 9413
[25] Massobrio C and Pasquarello A 2007 unpublished
[26] Susman S, Volin K J, Montague D G and Price D L 1990 *J. Non-Cryst. Solids* **125** 168
[27] Bhatia A and Thornton D 1970 *Phys. Rev.* B **2** 3004
[28] Waseda Y 1980 *The Structure of Non-Crystalline Materials* (New York: McGraw-Hill)
[29] Celino M and Massobrio C 2003 *Phys. Rev. Lett.* **90** 125502